Mechatronics 24 (2014) 1178–1188

Contents lists available at ScienceDirect

Mechatronics

journal homepage: www.elsevier.com/locate/mechatronics

A quad-rotor system for driving and flying missions by tilting mechanism of rotors: From design to control

S.H. Jeong, S. Jung *

Intelligent Systems and Emotional Engineering Lab., Department of Mechatronics Engineering, CNU, Republic of Korea

ARTICLE INFO

Article history:
Received 2 February 2013
Accepted 15 September 2014
Available online 4 November 2014

Keywords:
Quad-rotor system
Driving and flying control
Tilting mechanism of a rotor
Sensor fusion

ABSTRACT

This article presents the hybrid design and control of a quad-rotor system called Flymobile. Flymobile is a combined system of a mobile robot and a quad-rotor system aimed to perform both flying and driving tasks. Flymobile performs flying tasks in the same way as conventional quad-rotor systems while the tilting mechanism of each rotor allows Flymobile to navigate in its terrain for a driving task. The body frame with rotors is implemented by a calibration process through a test-bed equipped with a force sensor. The triangular wheel frame is designed to mimic motions of a mobile robot with three passive wheels. Sensor data of a gyro and an accelerometer are filtered and used for controlling the attitude of the system. Focusing on a practical approach of implementing a hybrid system, a non model-based approach is applied to control Flymobile. Experimental studies are demonstrated to show the feasibility of performing both driving and flying missions.

1. Introduction

Recently, research interest in unmanned aerial vehicles (UAVs) has been enormously increased. Successful missions performed by UAVs in the war zone as a military weapon have accelerated research in UAVs in many countries. Most of successful UAVs have a conventional take-off and landing (CTOL) structure that is suitable for a long range plan such as a surveillance task at remote areas. UAVs with the CTOL structure do not concern about the space for take-off and landing since they require enough space in wide areas.

In other aspects, however, UAVs can also be used for surveillance tasks in urban areas where a lot of buildings are surrounded. UAVs are often required to navigate between buildings to obtain information. This leads to the priority of using a vertical take-off and landing (VTOL) structure of UAVs. One of UAVs with the VTOL structure is a helicopter that has been around for many years [1–5]. Miniature design of mimicking a single rotor system has been introduced [5]. Although helicopters have great advantages of VTOL and hovering posture, an abrupt change of direction is not easily maneuvered and even of danger. Moreover, the backward movement of a helicopter is difficult from the hovering posture since it is not designed for omnidirectional movements in the sky.

Since the omnidirectional movement is preferred in the narrow space, quick movements help UAVs to improve maneuvering performances greatly. This requirement leads to the usage of a quad-rotor system that has four symmetrical rotors. Using four rotors provides several advantages. Firstly, hovering control performance can be achieved more easily than a single rotor system. This enables quad-rotors to cooperate each other for carrying objects together [4]. Secondly, control of quad-rotor systems is much easier than that of a single rotor system. Movements of a quad-rotor system are generated by controlling the velocity of each rotor instead of controlling the blade. This leads to an omnidirectional structure. Thirdly, payload to lift and carry objects can be increased since more rotors are used.

In the framework of the quad-rotor system design, many control algorithms have been proposed through simulation studies [6–16]. A nonlinear control method [6], a simple linear control method [7], and an inverse dynamics control method are applied to improve control performances [9]. Intelligent control approaches using neural network have been presented as well [12,14].

In practice, physical quad-rotor systems are developed and presented [17–26]. A quad-rotor system is controlled on the test-bed with a quaternion-based feedback control scheme [18]. Aggressive maneuvering control has been demonstrated based on PIDA controllers [20]. Recent research on quad-rotor systems is focused more on autonomous navigation through localization with the help of sensor fusion [21] and vision information [22–26].

* Corresponding author. Tel.: +82 42 821 6876; fax: +82 42 823 4919.
E-mail address: jungs@cnu.ac.kr (S. Jung).

http://dx.doi.org/10.1016/j.mechatronics.2014.09.006
0957-4158/

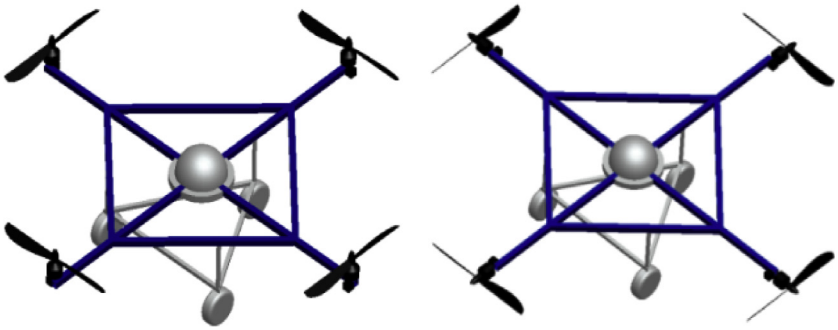

(a) Flying mode concept (b) Driving mode concept

Fig. 1. Design concept of Flymobile.

All of aforementioned research topics are concerned about the flying capability of quad-rotor systems. Both driving and flying operations of a quad-rotor system are rarely considered [27–29].

In this article, therefore, a novel hybrid design concept of a quad-rotor system having both flying and driving capabilities is presented [30]. The design concept of Flymobile for flying and driving is shown in Fig. 1. Each rotor can be tilted up for the flying mode as in Fig. 1(a), and is stretched out for the driving mode as in Fig. 1(b). For a driving capability, the base of the wheel frame is designed as a triangular shape which is easier to steer since it is constrained kinematically in the lateral direction.

A gyro and an accelerometer are used for detecting angles and output signals are filtered out by the complementary filter and the Kalman filter. Filtered signals are used for linear controllers to regulate the velocity of each rotor for attitude control. Calibration of making each rotor's force even by using a force sensor is performed. Each rotor having a tilting mechanism enables both driving and flying capabilities.

Since a practical approach of implementing a hybrid quadrotor system is focused, a non model-based control method is applied. Control gains are selected by empirical studies. Experimental studies of both flying and driving tasks of Flymobile are performed to demonstrate the feasibility of the concept of a future flying automobile.

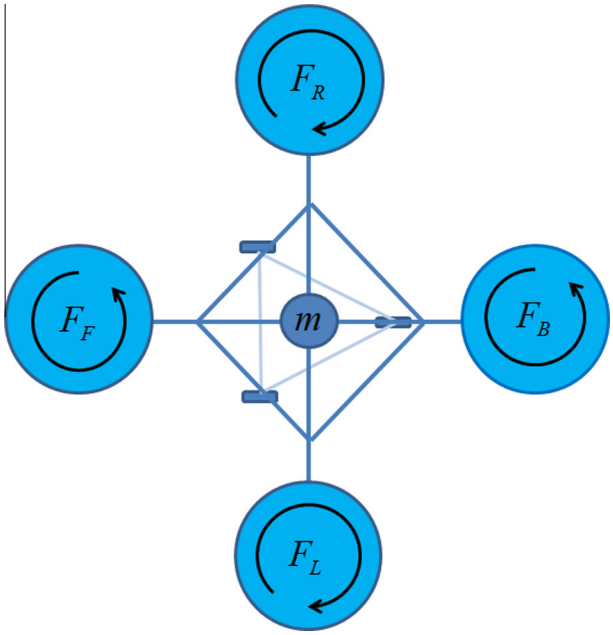

Fig. 2. Flying operation of Flymobile.

2. Operation of a quadrotor system

2.1. Flying operation

Flymobile has a symmetrical structure and four rotors are assumed to produce an equal thrust force as shown in Fig. 2. A pair of front (F) and back (B) rotors rotates in the counterclockwise direction and a pair of left (L) and right (R) rotors rotates in the clockwise direction to prevent the body from rotating. Directional movements can be generated by combining thruster forces induced by each rotor.

Table 1 lists the operational patterns of all directional flying movements of Flymobile. For example, Flymobile can fly up by summing the velocity of each rotor under the assumption that the characteristic of each rotor is same.

2.2. Driving operation

Using the concept of a mobile robot, three passive wheels are formed a triangle so that a driving operation can be defined as in Fig. 3. Flymobile navigates by a combined force of each rotor. The back wheel is a pin jointed and two front wheels are omni-directional so that the heading angle can be changed by rotors.

The driving operation is somewhat different from the flying operation listed in Table 1. To move forward as described in Fig. 3(a), the back force F_B is required to be smaller than the front force F_F and vice versa for the backward movement. Turning operations are different from the flying operation. To make the right turn, the left force F_L is chosen to be smaller than the right force F_R to push the body to the right as shown in Fig. 3(c) and vice versa for the left turn as in Fig. 3(d). Table 2 lists the driving operations of

Table 1
Flying motion command by rotor speed control.

	Front rotor F_F	Right rotor F_R	Back rotor F_B	Left rotor F_L
Move up	⇑	⇑	⇑	⇑
Stationary	↑	↑	↑	↑
Move down	^	^	^	^
Move forward	⇑	↑	^	↑
Move backward	^	↑	⇑	↑
Move left	↑	^	↑	⇑
Move right	↑	⇑	↑	^
Turn left	⇑	^	⇑	^
Turn right	^	⇑	^	⇑

(Relative scale: ⇑ > ↑ > ^).

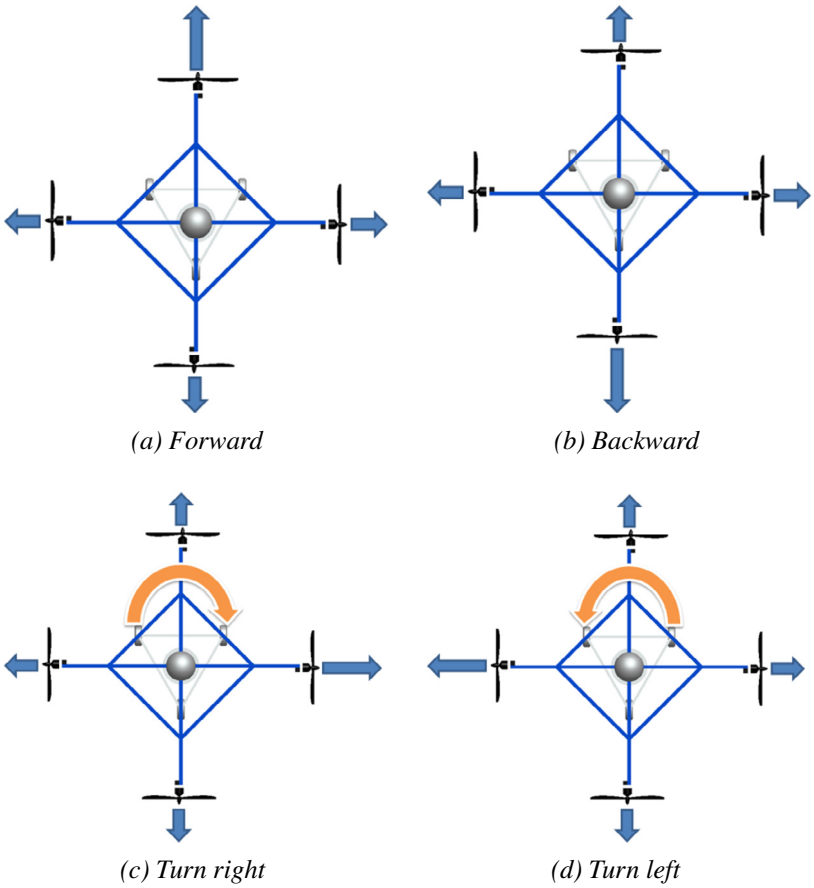

Fig. 3. Driving operation of Flymobile.

Table 2
Driving motion command by rotor speed control.

	Front rotor F_F	Right rotor F_R	Back rotor F_B	Left rotor F_L
Move Forward	⇑	↑	^	↑
Move Backward	^	↑	⇑	↑
Turn right	↑	⇑	↑	^
Turn left	↑	^	↑	⇑

(Relative scale: ⇑ > ↑ > ^).

Flymobile that show the relative magnitude scale of the thrust force of each rotor.

3. Control schemes

There are two strategies of controlling quadrotor systems, one is a model-based control approach and another is a non model-based approach. Although the non model-based approach requires more experimental exercises, it has great advantages of simplicity in controller design and dynamic analysis. Therefore, our concern

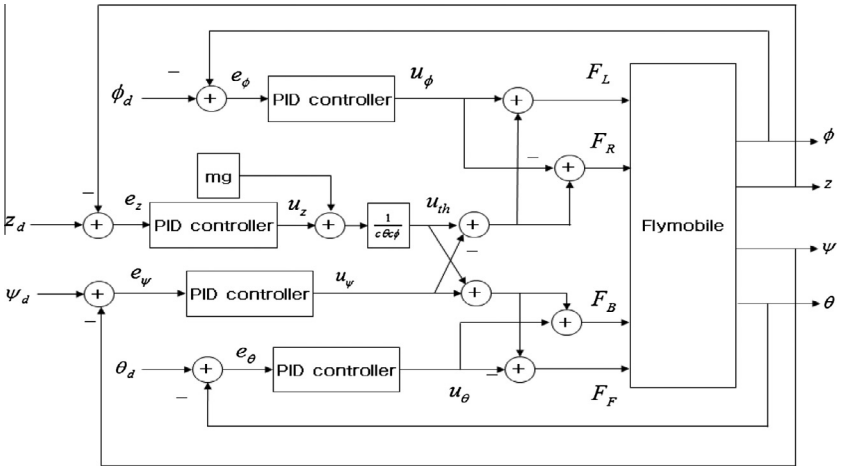

Fig. 4. Control block diagram.

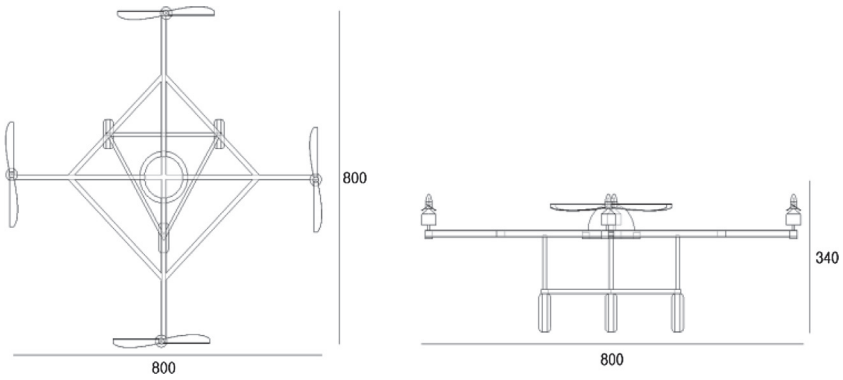

(a) Top view (b) Side view

Fig. 5. Body design.

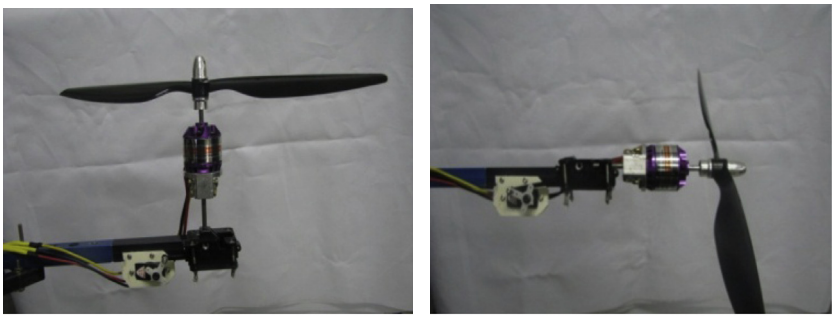

(a) Tilted up for flying (b) Tilted down for driving

Fig. 6. Tilting mechanism.

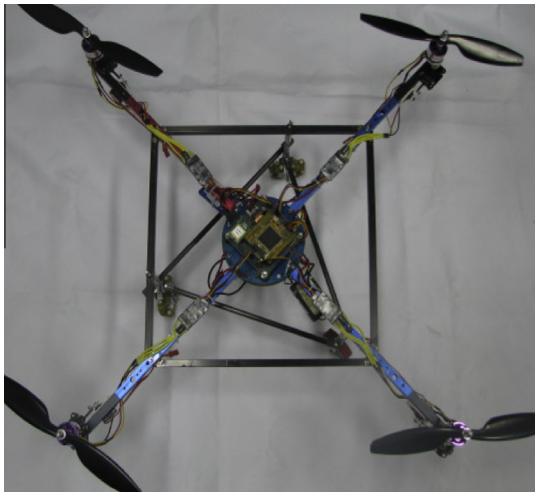

Fig. 7. Real Flymobile.

here is to control Flymobile without deriving dynamics of the system.

3.1. Angle control

Since Flymobile is an under-actuated system, we can only control four thrust forces from four rotors. Combined forces of each thrust force control variables such as three angles ϕ, θ, ψ and the altitude z to generate six motions in the space.

Control inputs for the roll, pitch, and yaw angle control are given below.

Table 3
Specifications of Flymobile.

Specifications	Units
Mass (m)	1.6 kg
Distance between Rotor and COG (l)	0.4 m
Maximum payload	2.5 kg
Length	0.8 m
Width	0.8 m
Height	0.34 m
MCU	DSP28335
Remote control	RF
Sampling time	2 ms

$$\begin{aligned} u_\phi &= k_{p\phi}(\phi_d - \phi) + k_{i\phi}\int(\phi_d - \phi)dt + k_{d\phi}(\dot{\phi}_d - \dot{\phi}) \\ u_\theta &= k_{p\theta}(\theta_d - \theta) + k_{i\theta}\int(\theta_d - \theta)dt + k_{d\theta}(\dot{\theta}_d - \dot{\theta}) \\ u_\psi &= k_{p\psi}(\psi_d - \psi) + k_{i\psi}\int(\psi_d - \psi)dt + k_{d\psi}(\dot{\psi}_d - \dot{\psi}) \end{aligned} \quad (1)$$

where $k_{p\phi}$, $k_{i\phi}$, $k_{d\phi}$ are PID controller gains for the roll angle control, $k_{p\theta}$, $k_{i\theta}$, $k_{d\theta}$ are PID controller gains for the pitch angle control, and $k_{p\psi}$, $k_{i\psi}$, $k_{d\psi}$ are PID controller gains for the yaw angle control.

3.2. Altitude control

The PID control method with the gravity compensation is used. We have the control law for the altitude control.

$$u_{th} = (u_z + mg)\frac{1}{\cos\theta\cos\phi} \quad (2)$$

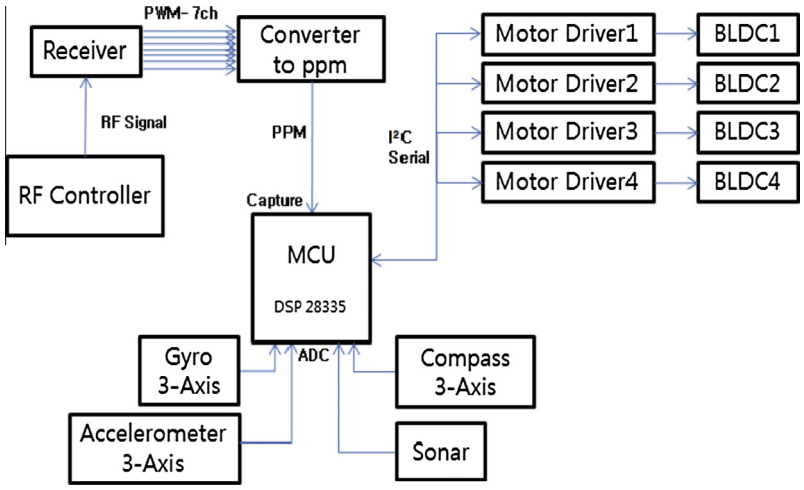

Fig. 8. Hardware structure.

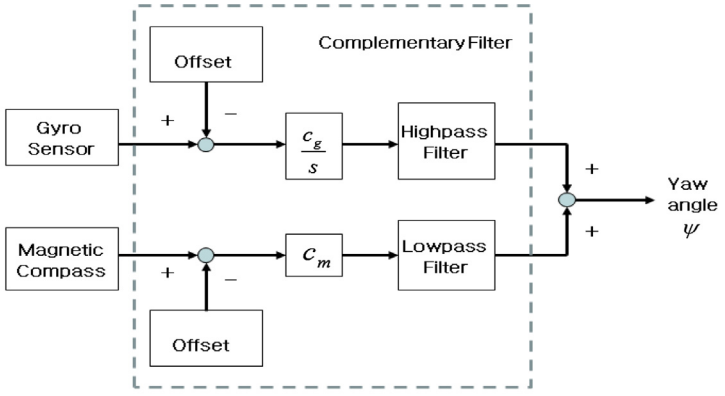

(a) Yaw angle estimation

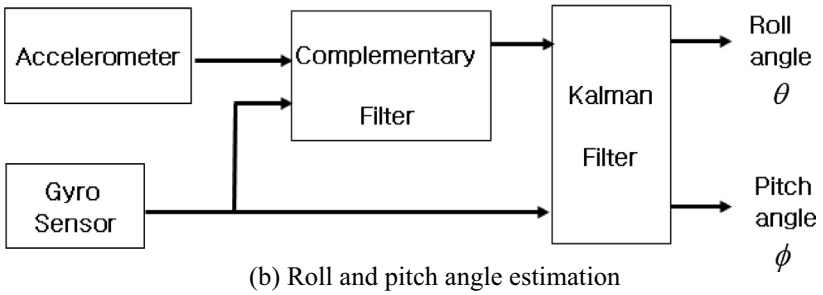

(b) Roll and pitch angle estimation

Fig. 9. Estimation of angle data.

where m is the mas, g is the gravitational acceleration, and u_z becomes

$$u_z = k_{pz}(z_d - z) + k_{iz}\int (z_d - z)dt + k_{dz}(\dot{z}_d - \dot{z}) \tag{3}$$

where k_{pz}, k_{iz}, k_{dz} are PID controller gains for the altitude control. The altitude data z can be obtained by a sonar sensor.

3.3. System output force

Each rotor output force is described by combining control inputs designed in (1)–(3). For example, if we add up the force F_i together, then we have the total thrust force u_{th} for the altitude control as shown in (3). Therefore, control input to each rotor can be given as

$$\begin{aligned} F_F &= au_{th} - bu_\theta - cu_\psi \\ F_B &= au_{th} + bu_\theta - cu_\psi \\ F_R &= au_{th} - bu_\phi + cu_\psi \\ F_L &= au_{th} + bu_\phi + cu_\psi \end{aligned}, \tag{4}$$

where $a = \frac{1}{4}, \quad b = \frac{1}{2L}, \quad c = \frac{1}{4C}$.

Fig. 4 shows the control block diagram for controlling three angles and the altitude of Flymobile.

4. Hardware design of flymobile

4.1. Schematic body design

The schematic body design of Flymobile is shown in Fig. 5. It has a squared rhombus frame whose each vertex is attached to one

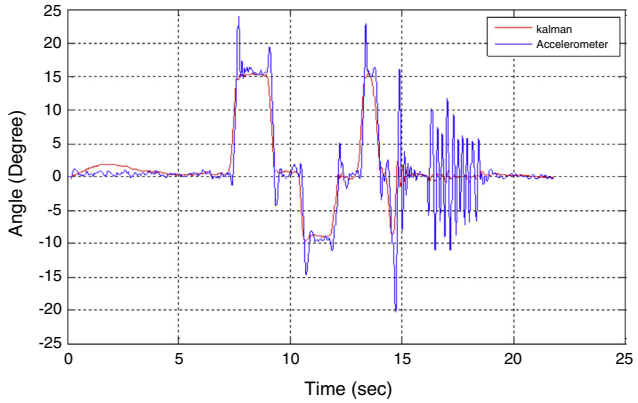

(a) Filtering results of Kalman filter and accelerometer

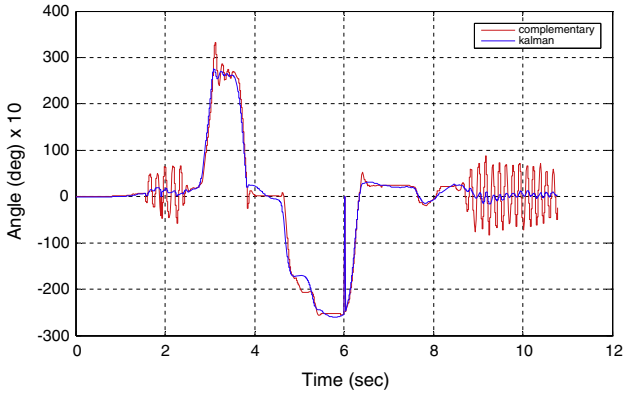

(b) Filtering of complementary and Kalman filters

Fig. 10. Sensor filtering results.

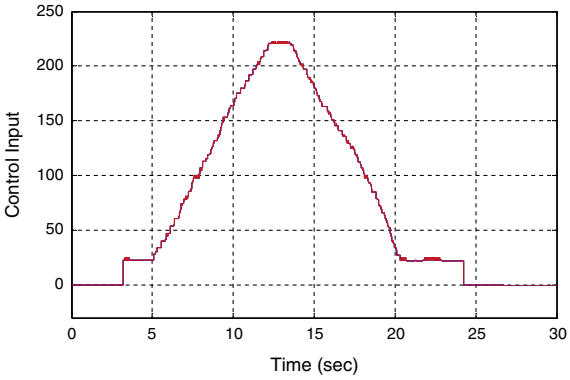

(a) Control input

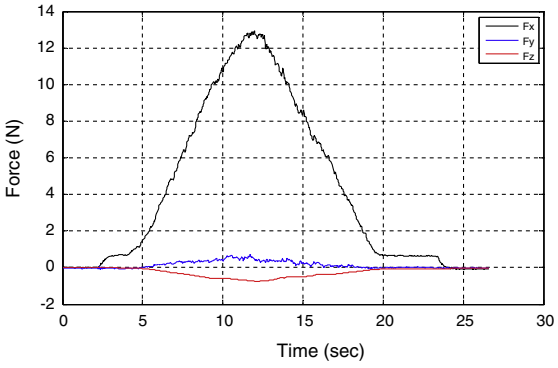

(b) X axis Force

Fig. 12. *X* axis force test by one rotor actuation.

rotor. Length and width form a square structure of 0.8(m) × 0.8(m) in a top view and its height is 0.34 m. The base frame with wheels forms a triangular shape, and each wheel is attached to each vertex. The triangular shape forms a wheeled-drive mobile robot.

4.2. Tilting mechanism

One of the main contributions is to develop hybrid design with the tilting mechanism of the Flymobile system. Each rotor has a tilting mechanism controlled by a servo motor. The tilting mechanism allows two operational modes: driving and flying mode as shown in Fig. 6. The flying mode can be achieved by tilting the rotor upward as in Fig. 6(a) and the driving mode by tilting the rotor downward as in Fig. 6(b).

4.3. Overall system

A real Flymobile system is shown in Fig. 7 as a top view. The mass is 1.6 kg and the length and width are 0.8 m to form a square. The maximum payload is 2.5 kg. The control sampling time is achieved at 2 ms. Table 3 lists the specifications of Flymobile.

One back wheel and two front omni-directional wheels are used for the mobile base. Different from the wheeled drive mechanism of mobile robots, front omni wheels are steered to change directions by rotors.

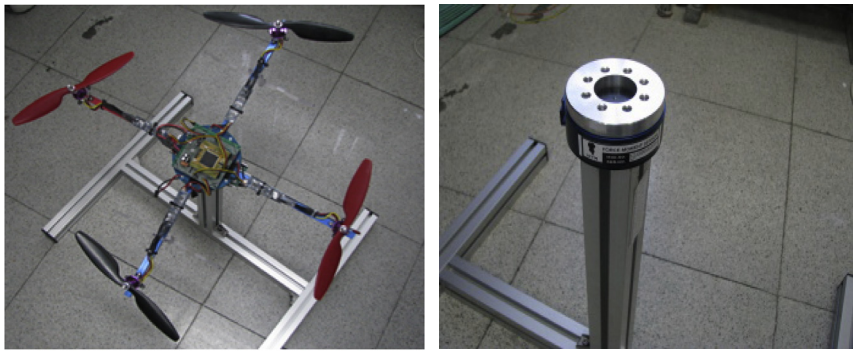

(a) Flymobile on the testbed (b) Force sensor

Fig. 11. Test-bed of the system.

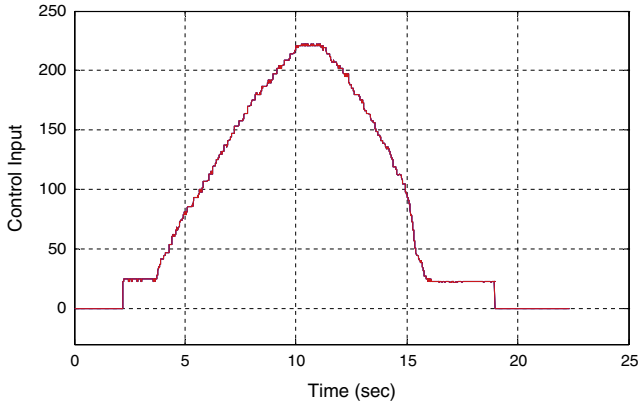

(a) Control input

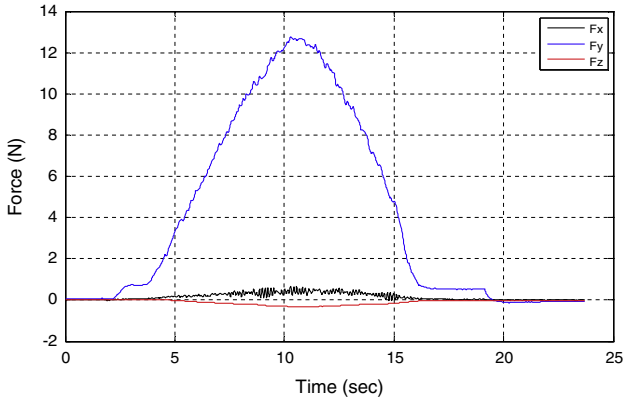

(b) Y axis force

Fig. 13. *Y* axis force test by one rotor actuation.

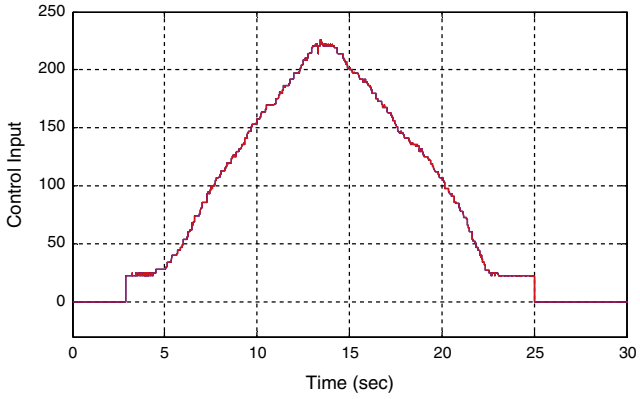

(a) X and Y axis control inputs

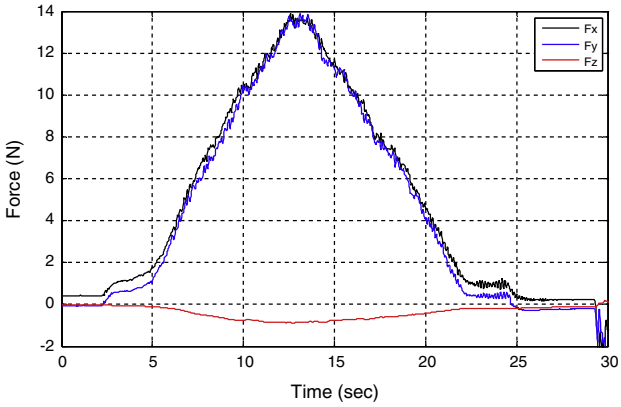

(b) X and Y axis forces

Fig. 14. *X–Y* axis force test by two rotors.

4.4. Hardware design

There are four rotors and corresponding drivers. A hardware structure is shown in Fig. 8.

The main controller is a DSP chip. A 3-axis gyro sensor, a 3-axis accelerometer, a sonar sensor, and a magnetic compass are used to detect the posture of the system. The gyro and accelerometer are used to detect the roll and pitch angle, and the magnetic compass is used for the yaw angle. The altitude from the ground is detected by the sonar sensor.

5. Calibrations

5.1. Attitude estimation

We estimate the yaw angle by using the 3-axis magnetic compass and 1-axis gyro information as shown in Fig. 9(a). We also measure and estimate roll and pitch angles using the 3-axis accelerometer and 2-axis gyro information as shown in Fig. 9(b). The sonar sensor is used for detecting the quad-rotor's altitude from the ground.

Roll and pitch angles are filtered by the complementary filter, and then by the Kalman filter to obtain more accurate signals. The Kalman filter equation is given as

$$x_{k+1} = \begin{bmatrix} 1 & -dT \\ 0 & 1 \end{bmatrix} x_k + \begin{bmatrix} dT \\ 0 \end{bmatrix} u_k + w_k$$
$$z_k = [\,1 \quad 0\,] x_k + v_k \tag{5}$$

where dT is a sampling time of 2 ms, $x_k = \begin{bmatrix} Angle\,predict \\ Gyro\,bias \end{bmatrix}$, $z_k = [Measured\_angle]$, $u_k = [Gyro\,rate]$, w_k and v_k are process noise and measurement noise, respectively.

Time update:

$$\hat{x}_k^- = A\hat{x}_{k-1} + Bu_{k-1}$$
$$P_k^- = AP_{k-1}A^T + Q \tag{6}$$

Measurement update:

$$K_k = P_k^- H^T (HP_{k-1}H^T + R)^{-1}$$
$$\hat{x}_k = \hat{x}_k^- + K_k(z_k - H\hat{x}_k^-) \tag{7}$$
$$P_k = (I - K_k H)P_k^-$$

where $A = \begin{bmatrix} 1 & -dT \\ 0 & 1 \end{bmatrix}$, $B = \begin{bmatrix} dT \\ 0 \end{bmatrix}$, $H = [\,1 \quad 0\,]$, and Q and R are covariance matrices of process and measurement noises, respectively.

We use the 3-axis gyro to detect 3-axis angular motions, two axes for the roll and pitch angles and one for the yaw angle. Since the yaw angle data of our sensor are quite noisy and inaccurate, we add the magnetic compass along with gyro information to estimate the yaw angle more correctly. Then signals are filtered out by the complementary filter as shown in Fig. 9(a).

The complementary filter combines two sensors of having different frequency responses and compensate for the lack of each sensor. The idea of the complementary filter is to use appropriate filters for typical sensor characteristics to suppress the corresponding noises. Further detailed implementation of the complementary filter can be found in [31]. The frequency of the low pass filter and the high pass filter is experimentally found and set to 1 Hz.

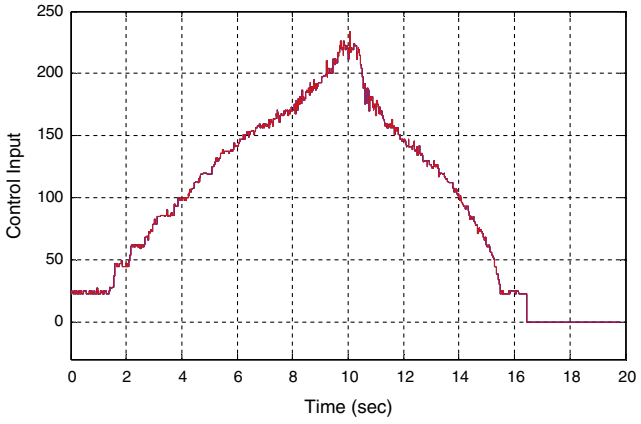

(a) Control input

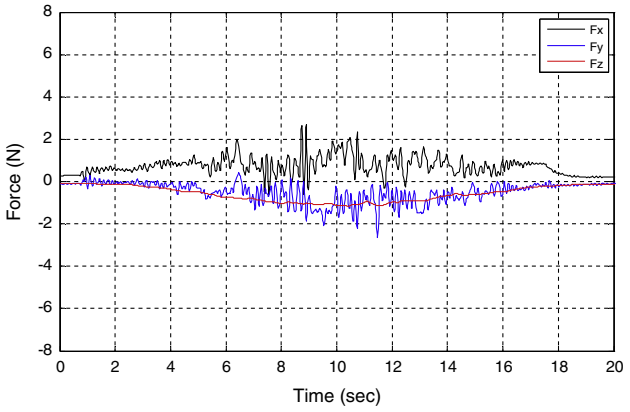

(b) Forces

Fig. 15. Force test by four rotors.

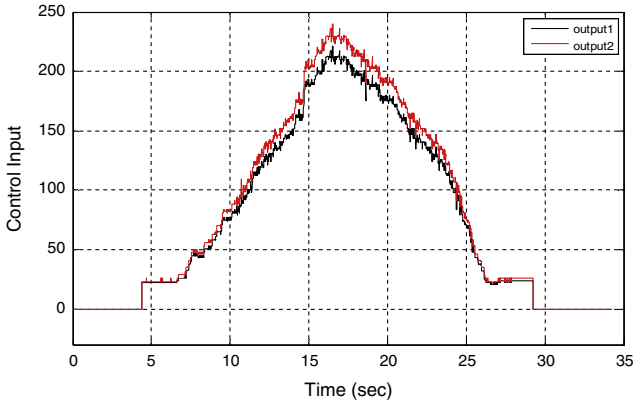

(a) Control inputs

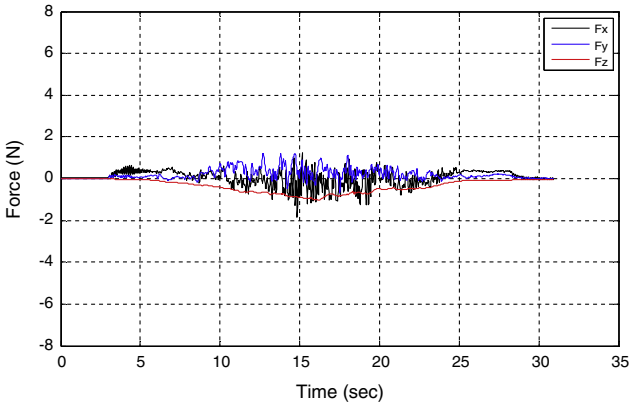

(b) Forces

Fig. 16. Calibrated force by four rotors.

Offset values in the complementary filter are obtained from empirical studies for calibration. C_g and C_m are tuning constants. Sensor algorithms are tested. Fig. 10(a) shows the filtering result after the Kalman filter over the accelerometer signals. Fig. 10(b) shows the sensor test result of the roll angle after both the Kalman filter and the complementary filter, which eliminates high frequency effects. Covariance values of Q and R for the Kalman filter are selected as Q_accelerometer = 0.00015, Q_gyro = 0.00015, and $r = 1$.

5.2. Calibration of rotors

Although each rotor is manufactured by the same company, each specification is slightly different. The same control input to each rotor may generate a different output force. This behavior clearly appears for the low cost motors. Asymmetrical frame structure appears although the center of the mass is assumed to be located on the center of the frame. Therefore, the calibration of each rotor is required to make the system symmetrical.

The overall test system is shown in Fig. 11. The whole system consists of Flymobile, a PC, a force sensor, and a test bed. Flymobile is located on the top of the test-bed which has a 6-axis force sensor.

5.2.1. Single rotor control

Firstly, the force of each axis by a single rotor is measured and calibrated. Fig. 12 shows the x axis force with respect to the control input and Fig. 13 shows the y axis force when one rotor is actuated.

(a) Flying mode

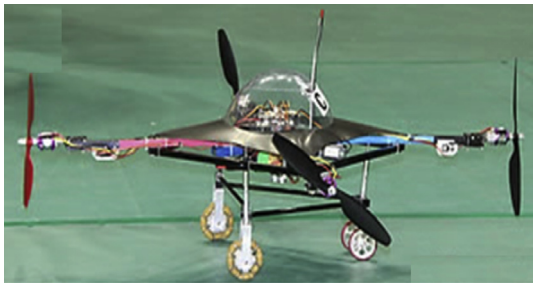

(b) Driving mode

Fig. 17. Flymobile demonstration.

Table 4
PID controller gains for experiment.

Gain	K_P	K_I	K_D
Roll ϕ	1.8	0.09	0.24
Pitch θ	1.8	0.1	0.27
Yaw ψ	0.8	0.01	0.5
Altitude z	0.014	0.0012	0.0018

(a) Hovering control demonstration

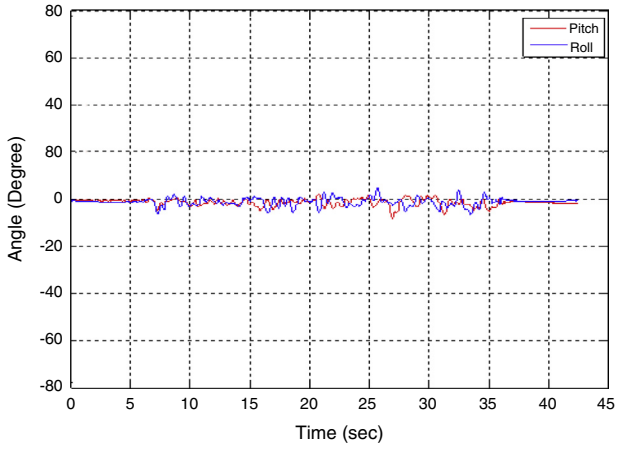

(b) Hovering data

Fig. 18. Outdoor hovering control demonstration.

5.2.2. Two-rotor control

Control inputs of two rotors are applied to the system and corresponding forces are measured. Fig. 14 shows x–y forces against the applied rotor actuation.

5.2.3. Four-rotor control

All four rotors are actuated. Since each rotor is assumed to be equal and to generate the equal force, the resulting force is expected to be zero in all directions. However, we see small deviations in force plots in Fig. 15. The error is about 2N. These errors are caused by several reasons such as an asymmetrical body frame, unbalanced fans, and different motor specifications.

Therefore, calibration process is required. Fig. 16 shows the force plots after adjusting outputs of each rotor to make about zero forces. Comparing Fig. 15(b) with Fig. 16(b), we clearly see that deviation errors are reduced in Fig. 16(b).

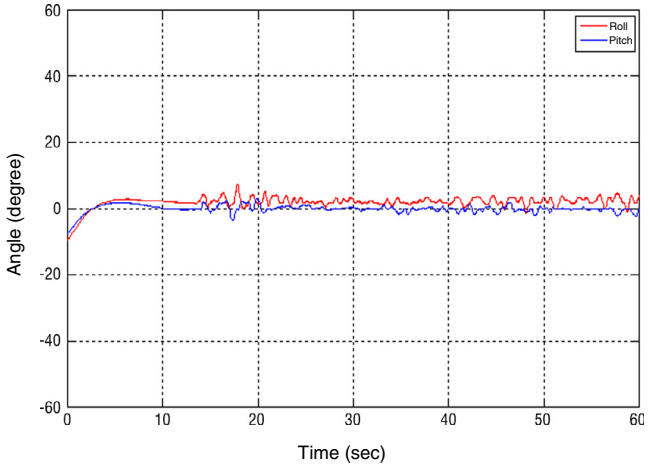

(a) Roll and pitch angle response

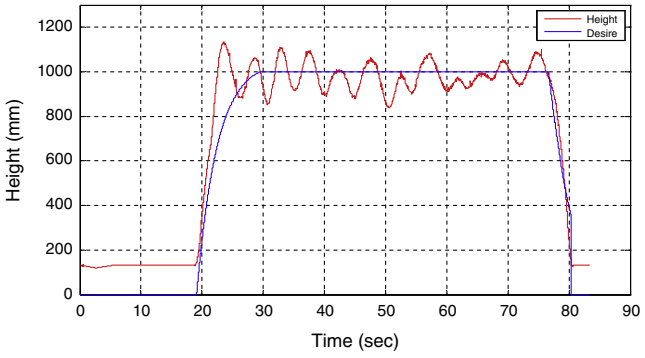

(b) Altitude control response

Fig. 19. Elevation altitude control demonstration.

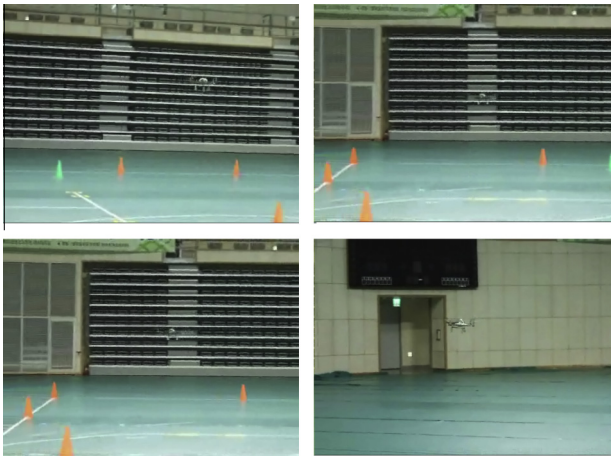

Fig. 20. Trajectory flying control demonstration.

6. Experimental studies

6.1. Hovering control

In experimental studies, two operational modes are tested. Flying and driving modes are separately tested as shown in Fig. 17(a) and (b), respectively. PID controller gains used for experimental studies are listed in Table 4. PID gains are obtained from empirical trial and error studies. In a practical system, control gains

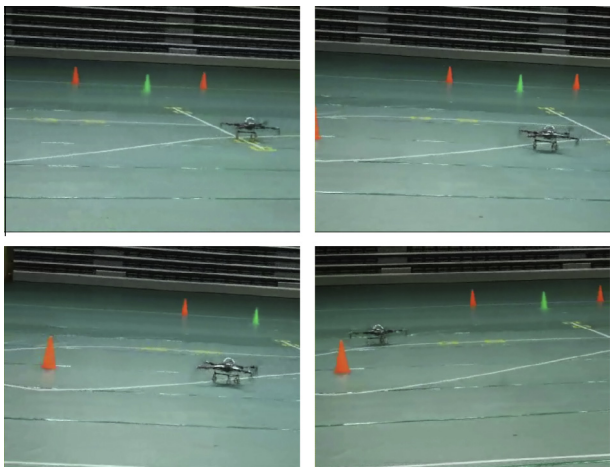

Fig. 21. Indoor driving control demonstration.

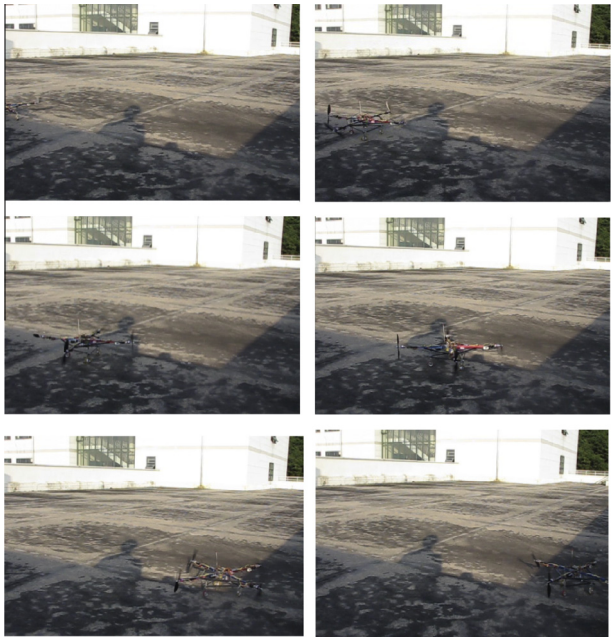

Fig. 22. Outdoor driving control demonstration.

are differently selected to improve the performance since the body is not exactly symmetrical.

Firstly, Flymobile is commanded to fly in the sky as commanded by the remote control through wireless communication. Initially, Flymobile is on the ground, and moves up slowly, then maintains for hovering motion at a certain height from the ground. Fig. 18 shows the hovering control demonstration on the roof of a building.

The corresponding angle plots are shown in Fig. 18(b). Pitch and roll angle errors are quite small and within ±3° which means that hovering control is well regulated.

6.2. Altitude control

Next experiment is the altitude control test. The desired altitude is given as 1 m from the ground. Fig. 19 shows plots of angle and altitude control responses. The distance from the ground is detected by a sonar sensor. Flymobile tries to maintain the desired altitude, but it shows oscillatory behaviors with the error bound of ±0.1 m. The corresponding roll and pitch angles are shown in Fig. 19(a). Roll and pitch angle errors are within ±3°. The roll angle error is relatively higher than that of the pitch angle since the altitude control shows the oscillatory behavior as shown in Fig. 19(b). Fig. 19(b) indicates that the sonar sensor is located at about 0.15 m from the ground of which the system height is 0.34 m. The rising time to reach at the desired altitude takes about 3 s.

6.3. Trajectory flying control

Flymobile is required to accomplish the flying mission of following the commanded trajectory in indoor environment. Fig. 20 shows the video-cut images of following the trajectory given in between cones. The operator controls the Flymobile remotely.

6.4. Driving control

The final experiment is the indoor and outdoor driving mode test. Movements of Flymobile on the ground are controlled by the operator though the remote controller so that desired trajectories are given by the remote controller. For an indoor driving test, Flymobile is required to follow the line on the floor through a remote control. Indoor line tracking demonstration is shown in Fig. 21.

Flymobile is also tested for outdoor driving on the roof of the building, of which surface is somewhat rough. Fig. 22 shows the video-cut images of the actual driving control test of following the circular trajectory from left to right. Although the surface is somewhat rough, driving movements of Flymobile are successfully demonstrated.

7. Conclusion

An interesting hybrid concept of a flying automobile has been presented by implementing a small-scaled Flymobile from design to implementation and control. Although Flymobile is driven by motors instead of engines, experimental studies can demonstrate the feasibility of a future concept car that can fly and run. Experimental studies confirm that Flymobile can fly and drive as commanded by the operator.

However, there are still several problems to be tackled. For the driving control, it is difficult for Flymobile to follow the desired trajectory exactly because it is a velocity-controlled system. To improve driving control performances, a braking mechanism for the wheels is required to regulate velocity more efficiently. For the flying control task, Flymobile should conduct missions such as surveillance or carrying objects which requires a camera and a GPS. Future research work should deal with aforementioned problems.

Acknowledgements

This work was supported in part by the 2012 Basic Science Research Program through the Korea Research Foundation funded by the Ministry of Science, ICT and Future Planning and the center for Autonomous Intelligent Manipulation (AIM) for service robots of the Ministry of Knowledge Economy (MKE) under the Human Resources Development Program for Convergence Robot Specialists support program supervised by the National IT Industry Promotion Agency (NIPA) under NIPA-2012-H1502-12-1002.

References

[1] McLean Donald. Automatic flight control system. Prentice Hall; 1990.
[2] Amaral TG, Crisostomo MM, Pires VF. Helicopter motion control using adaptive neuro-fuzzy inference controller. IEEE IECON 02, vol. 3; 2002, pp. 2090–5.

[3] Ferruz J, Vega VM, Ollero A, Blanco V. Reconfigurable control architecture for distributed systems in the HERO autonomous helicopter. IEEE Trans on Ind Electron 2011;58(12):5311–8.
[4] Eom IY, Jung S. A novel force tracking control approach to an autonomous unmanned helicopter system. IEEE IROS 2005:1027–32.
[5] Bouabdallah S, Becker M, Siewart R. Autonomous miniature flying robot: coming soon. IEEE Robot Automat Mag 2007:88–98.
[6] Xu R, Ozguner U. Sliding mode control of a quad-rotor helicopter. IEEE Conf Dec Control 2006:4957–62.
[7] Erginer B, Altug E. Modeling and PD control of a quad-rotor VTOL vehicle. IEEE Intelligent Vehicle Symposium; 2007, p. 894–99.
[8] Bouktir Y, Haddad M, Chettibi T. Trajectory planning for a quad-rotor helicopter. Mediterranean Conf Control Automat 2008:1258–63.
[9] Das A, Subbarao K, Lewis F. Dynamic inversion with zero-dynamics stabilization for quad-rotor control. IET Control Theory Appl 2009;3(3):303–14.
[10] Zhang R, Wang X, Cai KY. Quad-rotor aircraft control without velocity measurements. IEEE Conf Dec Control 2009:5213–8.
[11] Zuo Z. Trajectory tracking control design with a command-filtered compensation for a quad-rotor. IET Control Theory Appl 2010;4(11):2343–55.
[12] Dierks T, Jagannathan S. Output feedback control of a quad-rotor UAV using neural networks. IEEE Trans Neural Networks 2010;21(1):50–66.
[13] Meskin N, Khorasani K, Rabbath CA. A hybrid fault detection and isolation strategy for a network of unmanned vehicles in the presence of large environmental disturbances. IEEE Trans Control Syst Technol 2010;18(6):1422–9.
[14] Efe M. Neural network assisted computationally simple PID control of a quad-rotor UAV. IEEE Trans Ind Inform 2011;7(2):354–61.
[15] Zhang R, Quan Q, Cai KY. Attitude control of a quad-rotor aircraft subject to a class of time-varying disturbances. IET Control Theory Appl 2011;5(9):1140–6.
[16] Al-Younes YM, Al-Jarrah MA, Jhemi AA. Linear vs nonlinear control technique for a quad-rotor vehicle. International Symposium on Mechatronics and Its applications; 2010, p. 1–10.
[17] Castillo P, Dzul A, Lozano R. Real-time stabilization and tracking of a four-rotor mini rotorcraft. IEEE Trans Control Syst Technol 2004:510–6.
[18] Tayebi A, McGilvray S. Attitude stabilization of a VTOL quad-rotor aircraft. IEEE Trans Control Syst Technol 2006;14(3).
[19] Bouabdallah S, Siegwart R. Full control of a quad-rotor. IEEE Conf Intell Robots Syst 2007:153–8.
[20] Huang H, Hoffmann GM, Waslander SL, Tomlin CJ. Aerodynamics and control of autonomous quad-rotor helicopters in aggressive maneuvering. IEEE Conf Robot Automat 2009:3277–82.
[21] Grzonka S, Grisetti G, Burgard W. A fully autonomous indoor quad-rotor. IEEE Trans Robot 2011.
[22] Achtelik M, Zhang T, Kuhnlenz K, Buss M. Visual tracking and control of a quadcoptor using a stereo camera system and inertial sensors. IEEE Conf Mechatron Automat 2009:2863–9.
[23] Altug E, Ostrowski JP, Mahony R. Control of a quad-rotor helicopter using visual feedback. IEEE Int Conf Robot Automat 2002;1:72–7.
[24] Herrise B, Hamel T, Mahony R, Russotto F. Landing a VTOL unmanned aerial vehicle on a moving platform using optical flow. IEEE Trans Robot 2011.
[25] Guenard N, Hamel T, Mahony R. A practical visual servo control for an unmanned aerial vehicle. IEEE Trans Robot 2008;24(2):331–40.
[26] Schwager M, Jullian B, Angermann M, Rus D. Eyes in the sky: decentralized control for the deployment of robotic camera networks. Proc IEEE 2011;99(9):1514–6.
[27] Oner KT, Cetinsoy E, Unel M, Aksit MF, Kandemir I, Gulez K. Dynamic model and control of a new quad-rotor unmanned aerial vehicle with tilt-wing mechanism. World Acad Sci, Eng Technol 2008;45:58–63.
[28] Lee JO, Yoo CS, Park YS, Park BJ, Lee SJ, Gweon DG, et al. An experimental study on time delay control of actuation system of tilt rotor unmanned aerial vehicle. Mechatronics 2012.
[29] Cetinsoy E, Dikuar S, Oner KT, Sirimoglu E, Unel M, Aksit MF. Design and construction of a novel quad tilt-wing UAV. Mechatronics 2012;22:723–45.
[30] Jeong SH, Jung S. Novel design and position control of an omni-directional flying automobile (Omni-flymobile). ICCAS; 2010, p. 2480–4.
[31] Lee HJ, Jung S. Balancing and navigation control of a mobile inverted pendulum robot using sensor fusion of low cost sensors. Mechatronics 2012;22:95–105.